Research

Systematic Protein–Protein Interaction Analysis Reveals Intersubcomplex Contacts in the Nuclear Pore Complex*[S]

Luise Apelt‡, Kevin E. Knockenhauer§, Nina C. Leksa§, Nouhad Benlasfer‡, Thomas U. Schwartz§, and Ulrich Stelzl‡¶‖

The nuclear pore complex (NPC) enables transport across the nuclear envelope. It is one of the largest multiprotein assemblies in the cell, built from about 30 proteins called nucleoporins (Nups), organized into distinct subcomplexes. Structure determination of the NPC is a major research goal. The assembled ~40–112 MDa NPC can be visualized by cryoelectron tomography (cryo-ET), while Nup subcomplexes are studied crystallographically. Docking the crystal structures into the cryo-ET maps is difficult because of limited resolution. Further, intersubcomplex contacts are not well characterized. Here, we systematically investigated direct interactions between Nups. In a comprehensive, structure-based, yeast two-hybrid interaction matrix screen, we mapped protein–protein interactions in yeast and human. Benchmarking against crystallographic and coaffinity purification data from the literature demonstrated the high coverage and accuracy of the data set. Novel intersubcomplex interactions were validated biophysically in microscale thermophoresis experiments and in intact cells through protein fragment complementation. These intersubcomplex interaction data provide direct experimental evidence toward possible structural arrangements of architectural elements within the assembled NPC, or they may point to assembly intermediates. Our data favors an assembly model in which major architectural elements of the NPC, notably the Y-complex, exist in different structural contexts within the scaffold. ***Molecular & Cellular Proteomics 15: 10.1074/mcp.M115.054627, 2594–2606, 2016.***

Nucleocytoplasmic transport of molecules is universally mediated by nuclear pore complexes (NPCs)[1], ~40–112 MDa assemblies composed of ~ 30 different proteins (nucleoporins, or Nups). NPCs perforate the double-layered nuclear envelope. Because of an eightfold rotational symmetry around the central transport channel, each Nup is assumed to be present in multiples of eight copies, totaling ~500 individual proteins per NPC (1–3). Nups can be functionally classified: those with extended and presumed unstructured phenylalanine-glycine repeat elements that line the principal transport channel, those with membrane-interacting elements that anchor the NPC, and architectural Nups that form the principal NPC scaffold. Crystallographic studies of scaffold Nups have revealed that they are largely composed of β-propellers and stacked α-helical domain elements (4, 5). At least three architectural subcomplexes can be biochemically defined: the heteromeric Y-complex (6–10), the heteromeric (yeast) Nic96/(human) hsNup93 complex (11, 12) and the trimeric Nsp1/hsNup62 complexes (13–17).

The supramolecular structure of the NPC is intensively studied by cryoelectron tomography (cryo-ET), revealing distinct features characteristic for the cytoplasmic and nuclear side of the pore. Details of the scaffold ring structure are becoming apparent at ~2–6 nm resolution, in particular a distinction between three main elements—a central ring sandwiched between a cytoplasmic and a nucleoplasmic ring. Cumulative evidence from many experiments and laboratories suggests that the central ring is likely built by the Nic96/hsNup93 and the Nsp1/hsNup62 complexes, while both the cytoplasmic and nucleoplasmic rings of the scaffold are predominantly made up of Y-complexes.

Because of the resolution gap between the crystal structures and the tomographic reconstructions and an incomplete set of available crystal structures, obtained from a variety of evolutionarily distant species, docking approaches are still incomplete (9, 10, 18). This is further complicated by the paucity of intersubcomplex interaction data (12, 18–21).

From the ‡Otto-Warburg Laboratory, Max-Planck Institute for Molecular Genetics (MPIMG), Berlin, Germany; §Department of Biology, Massachusetts Institute of Technology (MIT), Cambridge; ¶Institute of Pharmaceutical Sciences, Pharmaceutical Chemistry, University of Graz, Graz, Austria

Received August 17, 2015, and in revised form, May 17, 2016
Published, MCP Papers in Press, May 17, 2016, DOI 10.1074/mcp.M115.054627
Author contributions: T.U.S. and U.S. designed research; L.A., K.E.K., N.C.L., and N.B. performed research; L.A., K.E.K., N.C.L., T.U.S., and U.S. analyzed data; T.U.S. and U.S. wrote the paper.

[1] The abbreviations used are: NPC, nuclear pore complex; Nups, nucleoporins; cryo-ET, cryoelectron tomography; HTP, highthroughput; PPI, protein-protein interaction; Y2H, yeast two-hybrid; ORF, open reading frame.

These interactions are presumably weak, highly dynamic, or both, thereby evading detection by typical approaches like copurification from fractionated cell extracts. Comprehensive binary protein–protein interaction information between Nups may thus be a critical piece of information in the determination of a high-resolution structural model of NPC.

Several technologies have been introduced for high-throughput (HTP) mapping of protein–protein interactions (PPIs), including affinity purification coupled to mass spectrometry and yeast two-hybrid (Y2H) assays. Using these HTP-PPI mapping approaches, relatively large proteomewide data sets have been generated (22). Also, more focused approaches were successful in systematically mapping specific cellular processes, selected functional groups of proteins, multiprotein complexes, or specific types of interactions (23, 24). Y2H approaches result in binary interaction information that is complementary to copurification-based approaches and thus often provide hints as to how complexes assemble or dynamically remodel in the course of cellular processes (25). Importantly, different HTP-Y2H setups, including ours, have been empirically assessed, demonstrating that PPI data sets are obtained with high precision (26).

In order to systematically study protein–protein interactions between all Nups, we performed a pairwise HTP-Y2H interaction screen involving yeast and human Nups, respectively. Our NPC interaction map recapitulated the intrasubcomplexes interactions with high coverage and additionally revealed several connections between Nups of distinct subcomplexes, *i.e.* intersubcomplex PPIs. The protein interaction map contains decisive information for structural model building of the NPC.

RESULTS

Comprehensive High-Resolution Y2H PPI Screening for Yeast and Human Nups—To better understand how Nups interconnect to build the NPC requires systematic analysis of binary PPIs between all Nups. Therefore, we set out to clone domain constructs as well as full-length open reading frames (ORFs) representing all Nups from yeast and human to perform a pairwise Y2H interaction analysis for the two species (Fig. 1). Because most Nups are soluble proteins, a stringent, well-controlled, high-quality Y2H approach is an optimal choice. Importantly, we wanted to obtain binary interaction information, including weak, more-transient association, which is best obtainable by Y2H analysis at large scale (26–28). Since all proteins used in the Y2H screen are *bona fide* NPC members, the search space to be examined is well defined and relatively small, thus the fraction of false positive interactions is expected to be very low.

In addition to the full length ORFs, we generated structure-based Y2H clones for yeast Nups (Supplemental Table S1), specifically removing phenylalanine-glycine repeat amino acid stretches that are thought to be aggregation prone and potentially more promiscuous in binding. The domain structure,

Group	Sc	Hs
Y-complex	Nup133 | 3	Nup133 | 6
	Nup84 | 1	Nup107 | 2
	Nup145C | 5	Nup96 | 1
	Sec13 | 1	Sec13 | 3
	Nup120 | 3	Nup160 | 2
	Nup85 | 3	Nup85 | 2
	Seh1 | 1	Seh1 | 4
		Nup43 | 4
		Nup37 | 3
Nic96 / Nup93 complex	Nic96 | 3	Nup93 | 2
	Nup59 | 1	Nup35 | 3
	Nup53 | 1	
	Nup188 | 3	Nup188 | 0
	Nup192 | 3	Nup205 | 0
	Nup170 | 3	Nup155 | 3
	Nup157 | 4	
Nsp1 / Nup62 complex	Nsp1 | 1	Nup62 | 4
	Nup82 | 2	Nup88 | 1
	Nup159 | 2	Nup214 | 0
	Nup57 | 1	Nup54 | 4
	Nup49 | 1	Nup58/NupL1 | 0
Linker Nups	Nup145N | 2	Nup98 | 1
	Nup100 | 2	
	Nup116 | 2	
Tm Nups	Ndc1 | 1	TMEM48 | 6
	Pom152 | 1	
	Pom34 | 1	
		Pom121 | 1
		Nup210 | 2
Basket	Nup2 | 2	Nup50 | 2
	Nup60 | 1	
	Mlp1 | 0	TPR | 1
	Mlp2 | 0	
Misc	Gle1 | 1	Gle1 | 0
	Gle2 | 1	RAE1 | 1
	Nup42 | 1	NupL2 | 2
	Mex67 | 1	
	Mtr2 | 1	
	Srp1 | 1	
	Yra1 | 1	
		AAAS | 5
Accessory	Gsp1 | 1	Ran | 0
	Kap95 | 1	
	Kap104 | 1	
	Kap114 | 1	
	Kap123 | 1	

FIG. 1. **Nuclear pore proteins of *S. cerevisiae* and *H. sapiens*.** Yeast (Sc) and human (Hs) homologous proteins are subdivided according to different substructures in the NPC (4) and color coded. Number of different constructs for a protein used in the study is given after the pipe (|).

based on crystallographic data and structure prediction, was considered in the design of protein fragment constructs. For instance, β-propeller domains were kept intact and α-helical domains designed matching existing structures. If crystal structures or homology models were unavailable, fragments were tested *in vitro* for acceptable chromatographic behavior. This approach should substantially decrease the number of false negatives and give rise to high-resolution information with regard to interacting protein domains. To study the binary interactions of human Nups, we subcloned full length cDNAs into Y2H vectors. In addition to covering 100 and 83% of the *bona fide* yeast and human Nups, respectively (29, 30), our clone sets also included accessory factors, like nuclear transport receptors and Ran. Including full-length proteins and structure-based fragments, the yeast set included a total of 66 constructs. 24 human Nups were covered with full-length clones (Fig. 1). 173 nonautoactive bait constructs (each protein as N-terminal and C-terminal DNA-binding domain fusion) and 128 prey constructs were examined six times in all possible pairwise combinations ($\sim$ 130,000 tests) (Fig. 2*A*). Considering only colonies that grew two or more times, the Y2H approach resulted in 79 interactions involving 14 human and 38 yeast constructs (Supplemental Table S1). While the various constructs provide more detailed information about binding regions, PPIs detected with multiple combinations of constructs and bait–prey configurations were combined into a data set that comprised 39 interactions between 25 yeast Nups, 15 interactions between 14 human Nups, and four cross-species interactions (Fig. 2*B*).

Validation of the NPC Y2H Data Set through Benchmarking—Several cocrystal structures of Nups have been determined and served as a standard for data comparison and benchmarking (Fig. 2*B*). Most of these structures are part of the stable Y-complex (Fig. 3*A*). Seven Y-complex interactions were recapitulated in the Y2H analysis: human (hs) hsNup133-Nup107; *Saccharomyces cerevisiae* (sc) scNup84–Nup145C; scNup145C–Nup85; scNup145C–Nup120; scNup120–Nup85; scNup145C–Sec13, and scNup85–Seh1. The conserved Y-complex scaffold is exactly reflected on the domain level in our data (Fig. 3*A*). For example, contacts revealed in the recent 4.1 Å Nup120–Nup145C-Sec13–Nup85 hub structure from *Myceliophthora thermophila* (9) and the 7.4 Å scNup120–Nup145C–Sec13–Nup85–Seh1–Nup84 structure (10) were recapitulated with corresponding protein domain constructs in our Y2H approach. The C-terminal 822–1037 amino acid part of scNup120 interacted with the scNup85 C-terminal tail domain (aa 533–744). It also interacted with the scNup145C tail domain. In contrast, the crown-trunk domain of scNup145C (aa 178–555) interacted with scNup84 (31, 32). The scNup85 tail (aa 533–744) also interacted directly with full-length scNup145C, as previously shown for various species (9, 10, 33). Four additional complexes for which crystal structures exist tested positive in our screen: scNsp1–Nup57; scNup57–Nup49; scNup82–Nup159; scNup82–Nup116 (34, 35) (Fig. 2*B*). Thus, our yeast PPI data provided complete coverage of the standard reference interactions derived from complex crystal structures, indicating that the NPC network contains highly reliable interaction information.

We next compared our data with two studies published by other labs that report binary interaction information between Nups. Leducq *et al.* (36) used a protein fragment complementation assay (PCA), based on the reconstitution of the enzyme dihydrofolate reductase, to assess interactions in two different yeast species. At the author's index value cut off, the resulting data set comprises 44 PPIs between 14 Nups for *S. cerevisiae* in the common interaction space and 12 interactions were found in the overlap (Fig. 2*B*). Amlacher *et al.* (37) investigated structural components of the NPC, namely members of the Y- and the Nic96-complexes, and performed a Y2H analysis on the respective proteins reporting 19 binary interactions, six of which are common to our data set (Fig. 2*B*). Thus, the overlap of our data was 13–16% with respect to the two other sets.

In a comprehensive study, Alber *et al.* (38) integrated ultracentrifugation, quantitative immunoblotting, coaffinity purification (co-AP), overlay assay, electron microscopy, immunoelectron microscopy, and fractionation data to produce an integrated structural model of the NPC. An interaction network defined through contact frequencies between Nups was calculated from the ensemble of optimized structures. Contact frequencies reflect the likelihood that a protein interaction is formed in the NPC, with values from 0–0.25, 0.25–0.75, and 0.75–1 binned as low, medium, and high frequencies (38). In agreement, a low fraction of our interactions was found to have low contact frequencies (15 of 296), and a high fraction of PPIs had high contact frequencies (8 of 26). Protein pairs with medium contact frequencies in the Alber data were also frequently found to interact (13 of 84) (Fig. 3*B*). However, the set of interactions with medium contact frequencies also contains five of the standard reference interactions from crystallization studies, suggesting that the importance of the medium frequency interactions may have been underestimated during the model building process.

Besides the integrative modeling approach taken, the co-AP approach by Alber *et al.* provided the most systematic PPI data set to date, reporting 82 affinity purifications of individually Protein A-tagged scNups (38). The protein composition of the purified complexes was resolved via SDS-PAGE/mass spectrometry analysis and composites covering all scNups were reported. These cocomplex data do represent completely independent PPI information but cannot be directly compared with our binary interaction data as such. For a comparison of our Y2H data with the co-AP data set, we transformed the composite matrix into a pairwise co-AP score weighting the number of co-occurrences of two proteins in a composite (25). Higher co-AP scores are given to protein pairs involving proteins that are found more rarely (*i.e.* in fewer complexes) and in more-stringent purification preparations

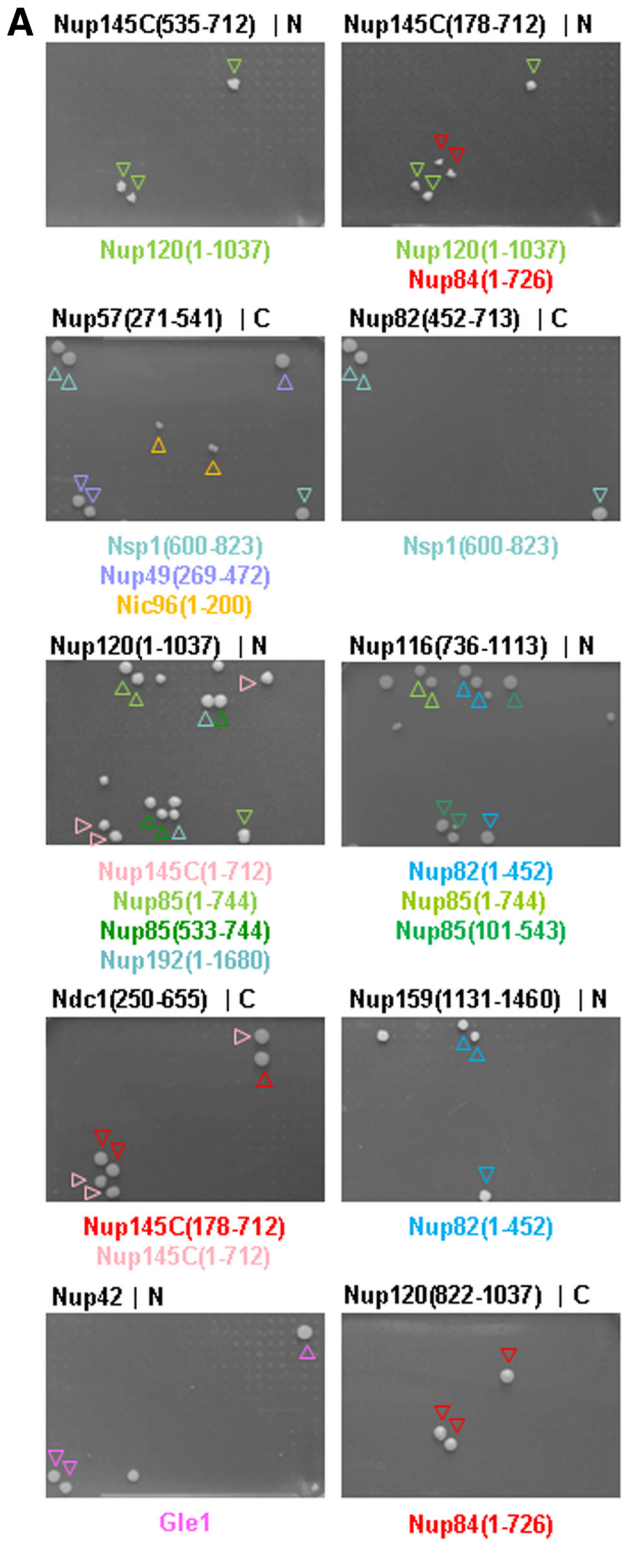

B

ProtA	ProtB	Y2H	Str	Aml	Led	CtcFreq	co-AP
Nup84	Nup145C	3	X	X		1.00	0.50
Nup84	Nup120	3				0.49	0.28
Nup145C	Sec13	3	X	X		0.50	0.45
Nup145C	Nup120	3	X		X	0.50	0.33
Nup145C	Nup85	3	X		X	0.35	0.33
Nup120	Nup120	3				nd	nd
Nup120	Nup85	3	X		X	0.60	0.35
Nup85	Seh1	2	X	X		1.00	0.61
Nup145C	Nup192	2				0.29	0.02
Nup120	Nup192	2				0.26	0.03
Nup145C	Nup82	1			X	0.17	0.03
Nup85	Nup82	2			X	0.19	0.02
Nup84	Nup100	3				0.03	0.05
Nup85	Nup100	3			X	0.02	0.00
Nup85	Nup116	3				0.05	0.02
Nup145C	Ndc1	3				0.11	0.00
Nic96	Nup59	2				0.44	0.07
Nic96	Nup53	3		X		0.23	0.08
Nup59	Nup192	3		X		0.56	0.18
Nup53	Nup192	3		X		0.28	0.10
Nic96	Nup57	1				0.42	0.35
Nup59	Nsp1	3				0.09	0.04
Nup59	Nup49	2				0.05	0.05
Nup53	Nup82	1				0.01	0.08
Nup188	Nup100	1				0.45	0.06
Nup188	Nup116	2				0.22	0.08
Nup192	Nup116	3				0.23	0.11
Nsp1	Nup82	3			X	1.00	0.37
Nsp1	Nup57	3	X		X	1.00	0.27
Nup82	Nup159	2	X		X	0.95	0.42
Nup82	Nup49	3				0.07	0.07
Nup57	Nup49	3	X		X	1.00	0.49
Nup82	Nup100	3			X	0.40	0.09
Nup82	Nup116	3	X		X	0.95	0.28
Nup49	Nup145N	2				0.04	0.00
Nup145N	Nup145N	3				nd	nd
Ndc1	Gle1	2				0.00	0.00
Nup2	Gsp1	2				nd	nd
Gle1	Nup42	3				1.00	1.00
hsNup133	hsNup107	3	X				
hsNup133	hsNup54	3					
hsNup133	AAAS	2					
hsNup133	RAE1	2					
hsSec13	hsSec13	3					
hsSec13	hsNup37	3					
hsSec13	hsSeh1	3					
hsSec13	hsNup62	1					
hsSec13	Pom121	1					
hsSec13	hsNupL2	1					
hsNup37	TPR	3					
hsNup54	hsNup62	2	X				
hsNup54	hsNup54	3					
hsNup54	Pom121	1					
hsNup93	hsNup35	2					
Nup145C	hsSec13	3	X				
Nup85	hsNup133	3					
Nup49	hsNup54	3					
Nic96	hsNup54	2					

FIG. 2. **Comprehensive Y2H screening of yeast and human Nups.** (*A*) Ten selective agar plates from the Y2H screens for the indicated sc-bait proteins (N- or C-terminal DNA binding domain fusion proteins, respectively), tested against a 384-prey plate with three independent colonies of every prey. Colony growth indicated an interacting bait–prey pair (colored arrow heads for sc-prey identity). Pairs that grew at least twice were considered for assembly of the final data set. (*B*) Summary of the Y2H interaction. Rows: Interacting yeast and human protein pairs (protein level) are listed. Sc-interacting pairs are separated from Hs-interacting pairs and four cross species sc-hs pairs. Columns: *Y2H,* Y2H

(*i.e.* in complexes with fewer proteins). Co-AP scores for all possible protein pairs were obtained ranging from 0 (proteins never purify together) to 1 (proteins exclusively purify as heterodimers, *e.g.* scNup42–Gle1). We then compared the co-AP scores with our Y2H data. The average co-AP score of the interacting pairs in our data set is much higher than in randomized networks with the same size and degree distribution, keeping the number of interactions for each protein constant (Fig. 3*C*, z-score = 6.6). For comparison, the average co-AP score for the data sets of Leducq and of Amlacher differed from their randomized networks too, albeit with smaller z-scores (z-score = 2.7 and 3.3, respectively, Supplemental Fig. S2). This indicates very good agreement of our binary Y2H data with the systematic co-AP study performed by Alber *et al.* (38), providing unbiased comprehensive validation of our data set.

The NPC PPI Network: Intra- and Intersubcomplex PPIs—Nups are largely conserved between human and yeast (Fig. 1*A*), and, though details will be species specific, it is assumed that the human NPC is similar to the yeast NPC both in its structural arrangement and in its overall shape (3, 39). Therefore, we investigated interactions of human and yeast Nups in parallel creating data that complement each other. The *Homo sapiens* Y2H network consists of 15 PPIs between 14 hsNups and is thus sparser than the yeast data set that comprises 39 PPIs between 25 scNups (Fig. 4). This was expected as only full-length human Nups were used in the analysis, which tend to be large and are therefore prone to yield false negative results. As proof in point, we did not obtain interactions for hsNup160 (162 kDa) and hsNup155 (155 kDa). On the other hand, three well-studied interactions were found in the human and the yeast screens: (i) the Y-complex interaction between hsNup133–Nup107 (7, 40, 41), (ii) the hsNup54–Nup62 and scNup57–Nsp1 interactions in the hsNup62/scNsp1-complex (15–17, 42), and (iii) the hsNup93–Nup35 interaction interolog to the scNic96–Nup53 interaction (37, 43). Similar to the hsNup133–Nup107 interaction that complemented the yeast network, additional human Nup interactions were found. Either the homologous interactions were not detected with the yeast proteins or the interactions involved proteins absent in *S. cerevisiae* such as the facultative Y-complex protein Nup37. For example, interactions between the β-propeller proteins hsSec13, hsSeh1, and hsNup37 were detected (Fig. 4).

Except for the scNup157/scNup170 orthologs, all yeast scaffolding Nups had at least one interaction in our network. In agreement with current interaction knowledge, more "intra" interactions, *i.e.* between Nups within one subcomplex, were found than "inter" interactions, *i.e.* between Nups of different subcomplexes. For example, in the yeast network three to four intra-Y-complex interactions are expected at random while the Y2H network contained nine PPIs (z-score = 5.4). Given the high (eightfold) symmetry of the NPC, homomeric interactions may be expected. While homomeric interactions systemically remain undetected in the published co-AP studies using haploid yeast strains (38), the Y2H approach has no such limitations. However, we still only found four homomeric interactions in total, scNup145N–Nup145N (C-term, aa 457–605), scNup120–Nup120 (N-term, aa 1–757), hsSec13–Sec13, and hsNup54–Nup54. The latter coiled–coiled interaction may well be detected only in the absence of hsNup58 and hsNup62, which together form a stoichiometric heterotrimeric complex (15–17).

The cytoplasmic and nucleoplasmic ring of the NPC are each considered to be primarily built by Y-complexes (1, 10, 18, 19), and they may serve as anchor points for complex assembly. Intersubcomplex interaction is critical to determine how the NPC assembles. We found connections from the scNup120 arm of the Y-complex to the Nic96/hsNup93 complex member scNup192 (Fig. 2*A*) and from scNup85 to scNup82, a component of the cytoplasmic filament network. The C terminus of scNup82 (aa452–713) was involved in an interaction with scNsp1 (Fig. 2*A*) (44), while the N-terminal β-propeller domain interacted with six other Nups, including the known interaction partners scNup159 and scNup116 (Fig. 2*A*) (35, 45, 46). The scNsp1 complex (Nsp1/Nup49/Nup57) (Fig. 2*A*) (47) connected to scNic96 (42) and scNup59. The three structurally similar phenylalanine-glycine -Nups (scNup100, scNup116, scNup145N) had interactions with members of the Y-, the Nic96, and the Nsp1 complex, as well as the cytoplasmic filament network. We did not find interactions between Y-complex members and the Nsp1 complex in yeast.

In an eightfold symmetrical NPC, every subcomplex is likely represented in multiples of eight (29, 48). Thus, in principle, some of the intracomplex interactions may contribute as intercomplex interaction in the assembled pore, but it is difficult to make this distinction from the Y2H interaction data alone. With the elucidation of the Nup120–Nup145C–Sec13–Nup85 Y-complex hub structure, it was possible to assemble a composite 3D atomic model of this subcomplex (9). Because our Y2H data perfectly reflect all interactions in the subcomplex at domain resolution (Fig. 3*A*), we can formally separate intra-Y-complex interactions from interactions that may occur in the pore between neighboring Y-complexes. Thus, in addition to the seven intra-Y-complex interactions,

score (1, 3) reflecting the success rate of how often a unique protein pair was found to interact in different replicas using different clones and different Y2H configurations. *Str,* X indicates that a crystal structure of the interacting pair has been determined (standard reference interaction set). *Aml,* X indicates an interaction reported by Amlacher *et al.* (37). *Led,* X indicates an interaction reported by Leducq *et al.* (36). *CtcFreq,* contact frequencies (medium shaded blue, high shaded green) reported by Alber *et al.* (38). *co-AP,* co-AP score (0. 00,1. 00] (25) derived from coaffinity purification (co-AP) experiments by Alber *et al.* (38).

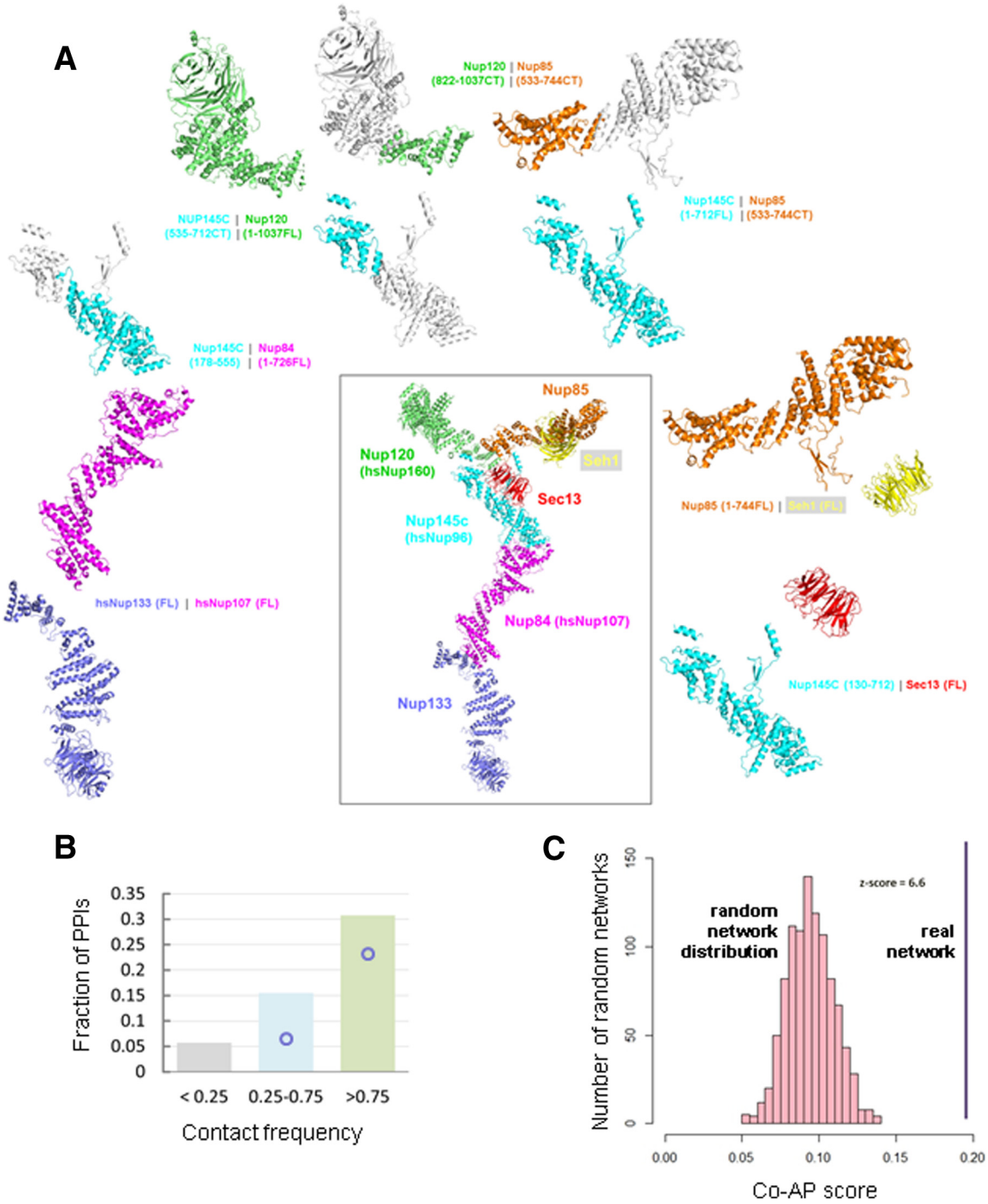

FIG. 3. **Validation of Y2H interaction through data comparison.** (*A*) Structural validation of Y2H interaction data. The inset shows the 3D composite color-coded structure model of the yeast heptameric Y-complex (9). All subunit interactions were recapitulated in the Y2H screen. Using several domain based constructs, minimal binding fragments were inferred from the Y2H data for yeast proteins and agree with the protein interfaces in the crystal structures. (*B*) Distribution of the fraction of interactions found with low (gray), medium (blue) and high (green) contact frequencies in Alber *et al.* (38). Fraction of interactions which were crystallized (standard reference interaction set) are indicated with blue circles. (*C*) Distribution of the number of randomized networks over their average co-AP score from 1000 randomizations. The value for the real network is 0.19 (blue line).

our Y2H analysis revealed two putative inter-Y-complex interactions in yeast: scNup84–Nup120 and scNup120–Nup120. Additionally, the cross human–yeast hsNup133–scNup85 C-terminal tail (aa 533–744) pair showed up most strongly in the Y2H analysis. The human data further revealed β-propeller—β-propeller interactions of hsSec13

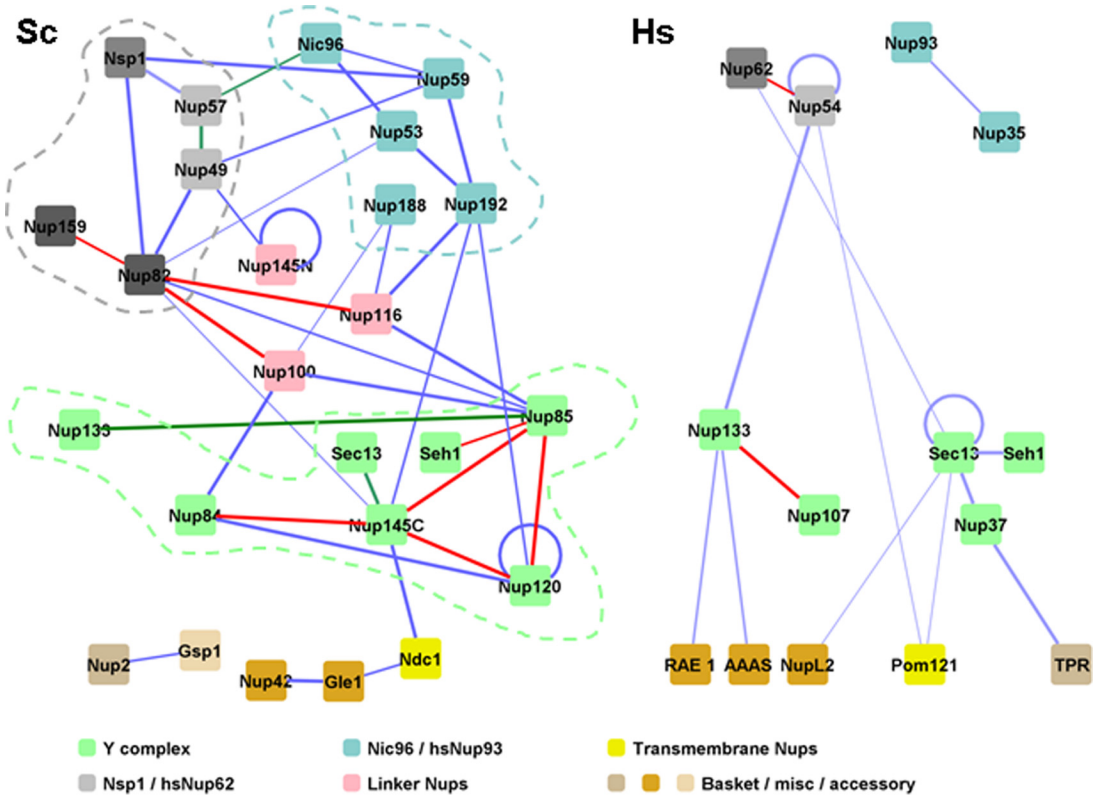

FIG. 4. **Network representation of the yeast and the human Y2H network, respectively.** The yeast PPI network is presented on the *left* and the human Y2H data on the *right*. Nodes indicate proteins, colored and grouped according to substructures. Edges indicate Y2H protein interactions, red: overlap with the standard reference set from x-ray structures, green: interactions that were also found cross species between human and yeast proteins.

with hsSec13, hsSeh1, and hsNup37 that also likely contribute inter-Y-complex interactions.

Biochemical Validation of Yeast Inter-Y-Complex PPIs—Many yeast Nups can be purified recombinantly from *Escherichia coli*. In particular, interacting members of the Y-complex can be copurified and used for *in vitro* binding measurements to validate novel inter-Y-complex interactions. We purified scNup120(1–757), scNup85/Seh1, scNup133(521–1157)/Nup84, and the scNup145C(34–712)/Nup120/Sec13 complex (31) via affinity chromatography followed by size exclusion chromatography to verify the three putative inter-Y-complex PPIs revealed in the Y2H analysis. We turned to microscale thermophoresis (MST), an approach that can monitor protein complex formation, as a binding partner typically alters the directed movement of a fluorescent protein through a microscopic temperature gradient in solution (49, 50). One protein was fluorescently labeled, kept at constant nM concentration, and the potential interaction partner was varied in concentration to measure apparent equilibrium binding constants (K_D). This approach does not require immobilization of one protein partner and thus eased problems arising from matrix-related background binding.

We could recapitulate the formation of the Y-complex hub with this setup. scNup145C(34–712)/Nup120/Sec13 and scNup85/Seh1 formed a complex with an apparent dissociation constant of $K_D \sim 0.15$ μM (Fig. 5*A*). We next tested scNup120 dimerization that was not detected during the purification procedure *e.g.* in the size exclusion chromatography step. However, scNup120 (aa 1–757) homodimer formation can be observed in the MST experiments and resulted in a dissociation constant in the lower micromolar range (Fig. 5*B*). Similarly, binding of labeled scNup120 (aa 1–757) with the scNup133(521–1157)/Nup84 complex was observed (Fig. 5*C*), matching the scNup120–Nup84 inter-Y-complex interaction proposed from the Y2H data. Finally, binding behavior was monitored when assaying labeled scNup85/Seh1 with increasing concentration of the scNup133(521–1157)/Nup84 complex. The concentration of the scNup133(521–1157)/Nup84 complex was limiting so that we did not reach full binding saturation in these experiments. However, a Δ Fnorm value range of ~20 AU (normalized fluorescence change = F_{hot}/F_{cold}) indicated binding (Fig. 5*D*). This experiment corroborated the scNup85–hsNup133 interolog. Dissociation constants in the low micrometer range are consistent with the idea that these interactions contribute to building the nuclear pore assembly from subcomplexes. Multiple contacts of proteins or subcomplexes within the NPC likely have an additive effect compared with the affinities of isolated components

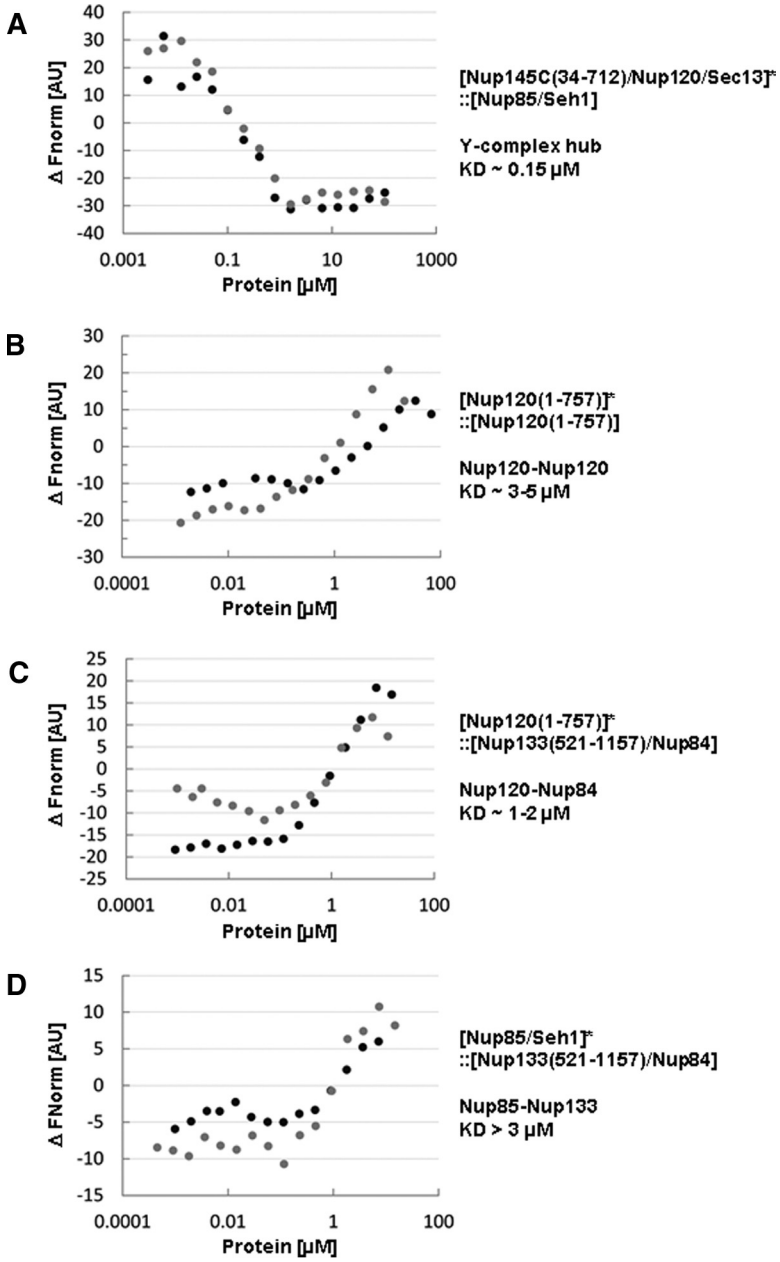

FIG. 5. **Microscale thermophoresis experiments to validate potential inter-Y-complex interactions.** (*A*) to (*D*) MST binding curves for the indicated protein interaction pairs. Δ Fnorm values were centered for every curve at 0. Protein complexes copurified from *E. coli* are indicated as well as the putative interacting proteins with their KD (apparent dissociation constant) values as determined from half saturation. While technical replicas, *i.e.* repetition of the MST binding curves with the same protein preparations typically result very similar curves, experiments performed with different protein preparations, in particular with independently labeled proteins are much more variable. Two independent binding curves are shown for each interaction.

measured *in vitro*. They may provide specificity while remaining more dynamic and susceptible to competition than more tight monovalent interactions (51).

Confirmation of Human β-Propeller and Inter-Y-Complex PPIs in Intact Human Cells—Six conserved proteins, scNup120/hsNup160, Nup133, scNup84/hsNup107, Nup85, scNup145C/hsNup96, and Sec13 together form two short arms and one long stalk, connected at a central hub, to build the Y-shaped complex (9). In addition to the conserved core proteins, the Y-complex can contain additional proteins, namely Seh1, Nup37, Nup43, or ELYS, depending on the species (52). The function of these accessory proteins is not yet fully understood (53). In the Y2H analysis of the human proteins, we found four interactions with hsSec13, the conserved β-propeller with a central position in the hub of the Y-complex. hsSec13 interacted with hsNup62, and with three other β-propeller proteins: hsSeh1, hsNup37, and hsSec13 itself.

In order to test these interactions in intact U2OS cells, we employed a YFP-based protein complementation assay (PCA) (54–56). In this assay, a YFP-fluorescence signal is reconstituted from two YFP fragments that fold through interaction of the proteins fused to the F1-YFP (aa 1–158 of Venus YFP) and F2-YFP (aa 159–239 of Venus YFP) fragments, respectively. We demonstrated the intra-Y-complex interaction between hsNup133 and hsNup107 (7, 40, 41) in this system (Fig. 6*A*).

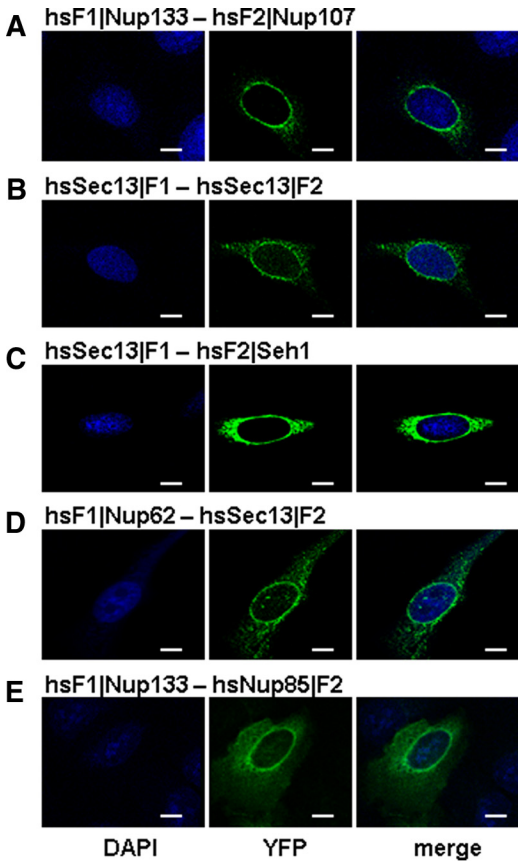

FIG. 6. **Protein complementation assays to validate potential inter-Y-complex interactions in intact human cells.** (*A*) to (*E*) Interacting protein pairs were expressed as YFP-F1 and YFP-F2 fusion proteins in U2OS cells. Cells were fixed and stained with DAPI (nucleus) and imaged for YFP-fluorescence by confocal microscopy. Nuclear rim staining indicates protein interaction in the NPC. (F1)Nup indicates a N-terminal F1-fragment fusion while Nup(F2) indicates a C-terminal F2-fragment fusion with the corresponding hsNup, respectively. Please note that combinations using the YFP-fragment fusion proteins from A to E did not result in recordable YFP fluorescence: hsF1 Nup133-hsSec13 F2; hsSec13 F1-hsF2 Nup107; hsF1 Nup133-hsF2 Seh1; hsF1 Nup62-hsF2 Seh1; hsF1 Nup62-hsF2 Nup107; hsSec13 F1-hsNup85 F2;. Scale bars: 10 μM.

Characteristic for proteins in the NPC, we observed YFP fluorescence at the nuclear rim in confocal images 36 h after transfection, recapitulating that hsNup133 and hsNup107 interact within the NPC. Complementation of hsNup133 or hsNup107 with either hsSec13, hsSeh1, or hsNup62 did not result any YFP signal, confirming the specificity of the test (Supplemental Fig. S3). HsSec13 interaction with hsNup62, hsSeh1, and hsSec13, as observed in the Y2H screen, were confirmed through protein fragment complementation localized mainly to the nuclear rim in intact human U2OS cells (Figs. 6*B*–6*D*). Besides the general assumption that the NPC is structurally similar between yeast and human, testing the hsNup133–scNup85 interaction provided further evidence that this interaction should be relevant in the human NPC. Assaying human Nup85 and Nup133 in our PCA approach, we observed a fluorescence signal at the nuclear rim (Fig. 6*E*). In addition to the biochemical interaction measurements with the yeast homologs (Fig. 5*D*), validation of this interaction in intact human cells seemed of particular interest providing a substantial constraint toward the arrangement of the Y-complexes with respect to each other within the nuclear pore complex.

DISCUSSION

The primary motivation for this study was to elucidate protein–protein interactions within the NPC that would provide a new basis for constructing composite assembly structures at high resolution. This is important because of the existing resolution gap between cryo-ET structures of the assembled NPC of different species. The supramolecular structure of the NPC of several species has been determined by cryo-ET at resolutions between ~7.6 and ~2 nm (3, 18, 19, 39, 57–60) and the growing, but still incomplete, list of available nucleoporin crystal structures does not yet allow for an unambiguous placement of all the components into a fully assembled NPC structure (20, 21).

Certain subcomplexes that organize the 30 nucleoporins are well understood. Because the components bind with high affinity, they can be more easily copurified and, for example, cocrystallized. The 7–10 membered Y-complex is the best example for a stable subcomplex (1, 8–10, 19, 61–63). Other interactions have been characterized as well but especially intersubcomplex interactions have been notoriously difficult to establish. Apparently, such contacts are either weak or are systematically missed by the respective assays. Here, we exploited structural knowledge of nucleoporins to design protein constructs for a comprehensive Y2H-based PPI analysis for the NPC. Specifically, unstructured domains were removed and constructs reflected structured, potential binding domains, such as β-propeller, stacked helical, coil–coil, and α/β domain arrangements. We assessed in a stringent pairwise Y2H matrix approach the NPC interactome for yeast and human and also examined cross-species interactions. Our data set describes 39 interactions between 25 yeast Nups and 15 interactions connecting human Nups. The substantially higher number of interactions we found between yeast Nups, using structured domains, relative to the human PPI, using full-length proteins, is explained by large proteins having a propensity to generate false negative results in Y2H, presumably for steric reasons. Benchmarking against other literature-derived data demonstrated the high quality of our data set. For example, pairs of proteins frequently copurifying in independent AP-MS analyses (1, 38) are highly enriched in our data (Fig. 3*C*). This suggests that overall, highly reliable interaction information was obtained in the approach providing useful leads for further investigation into how the NPC is assembled.

Largely due to the lack of reliable intersubcomplex interaction data, a number of rather tentative models for the NPC

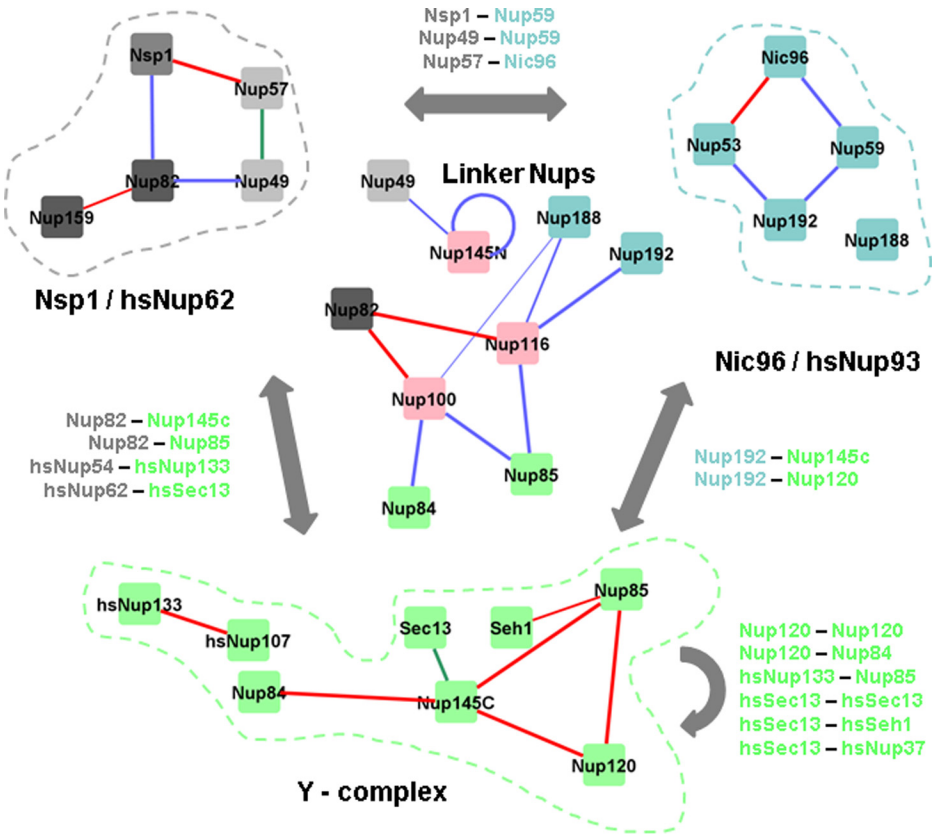

FIG. 7. **Interaction overview of the yeast Y2H interaction data emphasizing the modular structure of the NPC, showing intrasubcomplex and intersubcomplex interactions.** Edges indicate Y2H protein interactions, red: overlap with the standard reference set from x-ray structures, green: interactions that were also found cross species between human and yeast proteins.

assembly have been put forward over the years (1, 19, 64). The current benchmark, since based on a large body of experimental data and a ~3.2 nm cryo-ET map, is an assembly model first proposed by the Beck group (19). Because of the large size and distinct shape, the Y-complex is the prime substructure to be placed in the cryo-ET density map. Bui *et al.* posit that the Y-complex forms two eight-membered rings on the cytoplasmic as well as the nucleoplasmic side of the NPC, for a total of 32 copies per pore assembly. They suggest two reticulate rings in a head-to-tail orientation, where the Nup133 N-terminal β-propeller is the tail, while the hub area of the Y-complex defines the head. A central ring sandwiched between these two rings and assumed to primarily contain the hsNup93 subcomplex occupying the midplane of the NPC (20, 21).

One interesting question we asked is whether our PPI data are compatible with the two tandem ring model. For that, we focused on the inter-Y-complex interactions, which are Nup120 (aa 1–757)–Nup120 (aa 1–757), Nup120 (aa 1–757)–Nup84, Nup120 (aa 822–1037)–Nup84, Nup85 (aa 533–744)–hsNup133, hsSec13–hsSec13, hsSec13–hsSeh1, and, finally, hsSec13–hsNup37 (Fig. 7). Assuming all observed inter-Y interactions occur simultaneously in the assembled NPC, we have to conclude that several different Y-complex interfaces must exist, as all inter-Y contacts cannot coexist simultaneously in a single Y-complex pair conformation. For example, the Nup120–Nup120 and the Nup85–Nup133 are sterically prohibited from coexisting between two interacting Y-complexes, even when considering the considerable flexibility of the structure (9, 63, 65). This observation is in line with the tandem two-ring model that postulates at least four distinct microenvironments for Y-Y-complex contacts, *i.e.* each microenvironment has its specific set of interactions. That said, the interactions we see are only partially compatible with the two-ring model on a molecular level, assuming that the ring structure is generally conserved between human and yeast. While the Nup133–Nup85 contact is consistent with a possible inner ring Y–outer ring Y interaction, the Nup120–Nup120 interaction is in conflict with the tandem two-ring model because of an offset of ~12 nm of the inner ring/outer ring Y-complex pair. Equally, the hsSec13–hsSeh1 may contribute to conformational flexibility of the Y-complex hub (65), and the hsNup37–hsSec13 interaction may be involved in contacts by the neighboring inner- and outer-Y-complex, but coexistence with the hsSec13–hsSec13 contact is unlikely. However, to simply compare and contrast our putative inter-Y interactions with the assembly model for the NPC put forward by the Beck group would be overly simplistic. For instance,

hsSec13–hsSec13 and hsSec13–hsSeh1 may also be reflective of interactions within the GATOR2 (GAP towards Rags) complex where these proteins have an additional role (66). Also, major differences between the cytoplasmic and the nucleoplasmic rings cannot be ruled out at our current structural knowledge, as specifically discussed in the report of the latest cryo-ET structure of the *Xenopus* NPC (60).

Interactions between scaffold nucleoporins extending beyond the Y-complex have also been found. Many of them confirm previously established interactions (Fig. 7). Nup53 and Nup59 interacting both with Nic96 and Nup192 is consistent with a previously targeted Y2H analysis (37). The interaction between Nup82 and Nup159 as well as Nup82 and Nup100 or Nup116 is expected based on existing structural data (35). For the trimeric Nsp1 complex, we found direct contacts between Nup57 and Nsp1 and Nup57 and Nup49, as well as Nup57 and Nic96. These are consistent with the literature (15, 44, 67).

A number of additional contacts between NPC subcomplexes have been established (Fig. 7). Since the NPC is likely to be flexible on multiple levels (68), analysis of the interactome data is not trivial. As in the case of the Y-complex, flexibility is likely to create different microenvironments for other subcomplexes as well, such that detected interactions might only exist for a subset of Nups at any given time. Another point is that contacts that match established intrasubcomplex contacts could "hide" secondary, intersubcomplex interactions or be mutually exclusive. Further, the NPC needs to assemble into the confined space of the circular openings in the nuclear envelope. It is likely, although not tested, that the assembly process itself requires substantial conformational flexibility of subcomplexes. Therefore, an interaction detected in our screen may reflect a temporary contact with high relevance in the NPC assembly process, yet it may not occur in the completed NPC. Finally, it is becoming clear that the modular NPC can exist in different compositions, possibly to fulfill specialized functions (69, 70). Since our screen cannot differentiate between all these scenarios, the data may easily be overinterpreted. Despite these limitations, it is reasonable to assume that the interactome map is fairly comprehensive as it is a nearly complete coverage of previously known and structurally characterized interactions and thus provides a prime resource for pairwise interactions between Nups of the NPC.

MATERIALS AND METHODS

Y2H Screening—

Clones—Open reading frames (ORFs) were amplified via PCR and transferred to an Entry vector (pDONR221) in a BP cloning reaction. The ORFs were shuttled to Gateway destination vectors (*i.e.* lexA-[bait]: pBTM116-D9, pBTMcc24-DM; Gal4AD-[prey]: pACT4-DM; PCA Venus YFP-vectors: pVEN-F1C-DM, VEN-F2N-DM, pVEN-F2C-DM, pVEN-F1N-DM, F1: aa 1–158; F2: aa 159–239 of Venus YFP (71)) using standard procedures (Invitrogen).

Y2H Analysis—PPI matrix screening was performed as described previously (25, 28). In brief, nonautoactivating baits (L40ccU MATa yeast strains) were mated six times in 384-array format with prey strains using two and three independently transformed bait and prey yeast colonies, respectively. Interacting bait–prey pairs were identified by growth on selective agar plates (Leu-Trp-Ura-His). Only bait–prey pairs that showed growth at least two times were considered for further evaluation. As multiple clones and configurations of the same protein pair were tested in several replicas, we combined all data obtained for each interacting pair assigning a score (1, 3). The PPI data are reported in Table S1 and have been submitted to the IMEx (http://www.imexconsortium.org) consortium through IntAct (72) and assigned the identifier IM-25241.

Protein Purification—All protein constructs, from *S. cerevisiae,* were either expressed, in the case of Nup120(1–757), or coexpressed, in the case of complexes, with an N-terminal 10x-His tag from pET-Duet-derived plasmids in *E. coli* BL21 (DE3)-RIL. Cell growth, induction and nickel affinity purification steps were carried out as described in Kelley *et al.* (9). The nickel eluates were dialyzed overnight against 10 mM Tris/HCl (pH 8.0), 150 mM NaCl, 0.1 mM EDTA, and 1 mM DTT, in the case of Nup85/Seh1 and Nup145C(34–712)/Nup120/Sec13, or 10 mM potassium phosphate (pH 8.0), 150 mM NaCl, 0.1 mM EDTA, and 1 mM DTT, in the case of Nup120(1–757) and Nup133(521–1157)/Nup84. The 10xHis-tag was cleaved with 3C protease during dialysis. The proteins were further purified by ion exchange chromatography on a HiTrapQ column (GE Healthcare), for Nup85/Seh1 and Nup145C(34–712)/Nup120/Sec13, or a HiTrapS column (GE Healthcare), for Nup120(1–757) and Nup133(521–1157)/Nup84, using a linear NaCl gradient. The appropriate fractions were pooled and run on size exclusion chromatography using a Superdex S200 26/60 column (GE Healthcare) equilibrated in 10 mM Tris/HCl (pH 8.0), 150 mM NaCl, 0.1 mM EDTA, and 1 mM DTT. Proteins were concentrated to 2.6–29.5 mg/ml. The purity was assessed on SDS-PAGE.

Microscale Thermophoresis—Purified proteins were labeled following the manual of Nanotemper technology, *i.e.* Monolith NT™ Protein Labeling Kit BLUE-NHS 647. The concentration of labeled proteins was adjusted to ~50–100 nM. Dilution series of up to 16 unlabeled protein concentrations were prepared in a final volume of 20 μl for the MST measurements. Capillaries were filled and loaded into the Monolith NT.115, and the thermophoresis was performed using the Monolith NT.115 Nanotemper™ Technology.

Protein Complementation Assays in Mammalian Cells—U2OS cells were seeded in 24-well plates on cover slips and cotransfected with pairs of 50 ng Venus-F1 and 50 ng Venus-F2 plasmid DNA. 12–24 h after transection cell were grown further in fresh DMEM/FBS (5%) for additional 24 h. The cells were fixed at room temperature for 10 min in the dark with 2% paraformaldehyde in DPBS. Cells were stained with DAPI (16 μg/ml) for 2 min at room temperature. To visualize the YFP signal indicative of a protein interaction, a confocal fluorescence microscope (LSM700, Zeiss) at excitation wave length 525 nm was used.

Computational Analyses—Network analyses and visualization were performed with Cytoscape, R and custom PERL scripts for network link randomization procedures. Co-AP scores (25) were calculated using composite interaction profiles from Supplemental Fig. 4 of Alber *et al.* (38).

Acknowledgments—We thank Moran Jerabek-Willemsen (Nanotemper) for advice with MST experiments, Kotaro Kelley for help with protein purification, and Jonathan Woodsmith for critical reading of the manuscript.

* This work was supported by the Max Planck Society and the German Ministry of Science (NGFNp, NeuroNet-TP3 01GS08171; BMBF, 0315082) and the National Institutes of Health (T. U. S.,

R01GM77537; K. E. K. and N. C. L., T32GM007287). The funders had no role in study design, data collection and analysis, decision to publish, or preparation of the manuscript.

S This article contains supplemental material.

‖ To whom correspondence should be addressed: stelzl@molgen.mpg.de.

The authors declare that no competing interests exist.

REFERENCES

1. Alber, F., Dokudovskaya, S., Veenhoff, L. M., Zhang, W., Kipper, J., Devos, D., Suprapto, A., Karni-Schmidt, O., Williams, R., Chait, B. T., Sali, A., and Rout, M. P. (2007) The molecular architecture of the nuclear pore complex. *Nature* **450,** 695–701
2. Strambio-De-Castillia, C., Niepel, M., and Rout, M. P. (2010) The nuclear pore complex: bridging nuclear transport and gene regulation. *Nat. Reviews* **11,** 490–501
3. Grossman, E., Medalia, O., and Zwerger, M. (2012) Functional architecture of the nuclear pore complex. *Ann. Rev. Biophys.* **41,** 557–584
4. Brohawn, S. G., Partridge, JR, Whittle, JR, and Schwartz, T. U. (2009) The nuclear pore complex has entered the atomic age. *Structure* **17,** 1156–1168
5. Schwartz, T. U. (2016) The Structure Inventory of the Nuclear Pore Complex. *J. Mol. Biol.* **428,** 1986–2000
6. Siniossoglou, S., Wimmer, C., Rieger, M., Doye, V., Tekotte, H., Weise, C., Emig, S., Segref, A., and Hurt, E. C. (1996) A novel complex of nucleoporins, which includes Sec13p and a Sec13p homolog, is essential for normal nuclear pores. *Cell* **84,** 265–275
7. Belgareh, N., Rabut, G., Baï, S. W., van Overbeek, M., Beaudouin, J., Daigle, N., Zatsepina, O. V., Pasteau, F., Labas, V., Fromont-Racine, M., Ellenberg, J., and Doye, V. (2001) An evolutionarily conserved NPC subcomplex, which redistributes in part to kinetochores in mammalian cells. *J. Cell Biol.* **154,** 1147–1160
8. Lutzmann, M., Kunze, R., Buerer, A., Aebi, U., and Hurt, E. (2002) Modular self-assembly of a Y-shaped multiprotein complex from seven nucleoporins. *EMBO J.* **21,** 387–397
9. Kelley, K., Knockenhauer, K. E., Kabachinski, G., and Schwartz, T. U. (2015) Atomic structure of the Y complex of the nuclear pore. *Nat. Struct. Mol. Biol.* **22,** 425–431
10. Stuwe, T., Correia, A. R., Lin, D. H., Paduch, M., Lu, V. T., Kossiakoff, A. A., and Hoelz, A. (2015) Nuclear pores. Architecture of the nuclear pore complex coat. *Science* **347,** 1148–1152
11. Vollmer, B., and Antonin, W. (2014) The diverse roles of the Nup93/Nic96 complex proteins - structural scaffolds of the nuclear pore complex with additional cellular functions. *Biol. Chem.* **395,** 515–528
12. Fischer, J., Teimer, R., Amlacher, S., Kunze, R., and Hurt, E. (2015) Linker Nups connect the nuclear pore complex inner ring with the outer ring and transport channel. *Nat. Struct. Mol. Biol.* **22,** 774–781
13. Finlay, Meier, E., Bradley, P., Horecka, J., and Forbes, D. J. (1991) A complex of nuclear pore proteins required for pore function. *J. Cell Biol.* **114,** 169–183
14. Guan, T., Müller, S., Klier, G., Panté, N., Blevitt, J. M., Haner, M., Paschal, B., Aebi, U., and Gerace, L. (1995) Structural analysis of the p62 complex, an assembly of O-linked glycoproteins that localizes near the central gated channel of the nuclear pore complex. *Mol. Biol. Cell* **6,** 1591–1603
15. Ulrich, A., Partridge, JR, and Schwartz, T. U. (2014) The stoichiometry of the nucleoporin 62 subcomplex of the nuclear pore in solution. *Mol. Biol. Cell* **25,** 1484–1492
16. Chug, H., Trakhanov, S., Hülsmann, B. B., Pleiner, T., and Görlich, D. (2015) Crystal structure of the metazoan Nup62*Nup58*Nup54 nucleoporin complex. *Science* **350,** 106–110
17. Stuwe, T., Bley, C. J., Thierbach, K., Petrovic, S., Schilbach, S., Mayo, D. J., Perriches, T., Rundlet, E. J., Jeon, Y. E., Collins, L. N., Huber, F. M., Lin, D. H., Paduch, M., Koide, A., Lu, V., Fischer, J., Hurt, E., Koide, S., Kossiakoff, A. A., and Hoelz, A. (2015) Architecture of the fungal nuclear pore inner ring complex. *Science* **350,** 56–64
18. von Appen, A., Kosinski, J., Sparks, L., Ori, A., DiGuilio, A. L., Vollmer, B., Mackmull, M. T., Banterle, N., Parca, L., Kastritis, P., Buczak, K., Mosalaganti, S., Hagen, W., Andres-Pons, A., Lemke, E. A., Bork, P., Antonin, W., Glavy, J. S., Bui, K. H., and Beck, M. (2015) In situ structural analysis of the human nuclear pore complex. *Nature* **526,** 140–143
19. Bui, K. H., von Appen, A., DiGuilio, A. L., Ori, A., Sparks, L., Mackmull, M. T., Bock, T., Hagen, W., Andrés-Pons, A., Glavy, J. S., and Beck, M. (2013) Integrated structural analysis of the human nuclear pore complex scaffold. *Cell* **155,** 1233–1243
20. Kosinski, J., Mosalaganti, S., von Appen, A., Teimer, R., DiGuilio, A. L., Wan, W., Bui, K. H., Hagen, W. J., Briggs, J. A., Glavy, J. S., Hurt, E., and Beck, M. (2016) Molecular architecture of the inner ring scaffold of the human nuclear pore complex. *Science* **352,** 363–365
21. Lin, D. H., Stuwe, T., Schilbach, S., Rundlet, E. J., Perriches, T., Mobbs, G., Fan, Y., Thierbach, K., Huber, F. M., Collins, L. N., Davenport, A. M., Jeon, Y. E., and Hoelz, A. (2016) Architecture of the symmetric core of the nuclear pore. *Science* **352,** aaf1015
22. Woodsmith, J., and Stelzl, U. (2014) Studying post-translational modifications with protein interaction networks. *Curr. Opin. Struct. Biol.* **24,** 34–44
23. Weimann, M., Grossmann, A., Woodsmith, J., Özkan, Z., Birth, P., Meierhofer, D., Benlasfer, N., Valovka, T., Timmermann, B., Wanker, E. E., Sauer, S., and Stelzl, U. (2013) A Y2H-seq approach defines the human protein methyltransferase interactome. *Nat. Methods* **10,** 339–342
24. Grossmann, A., Benlasfer, N., Birth, P., Hegele, A., Wachsmuth, F., Apelt, L., and Stelzl, U. (2015) Phospho-tyrosine dependent protein–protein interaction network. *Mol. Syst. Biol.* **11,** 794
25. Hegele, A., Kamburov, A., Grossmann, A., Sourlis, C., Wowro, S., Weimann, M., Will, C. L., Pena, V., Lührmann, R., and Stelzl, U. (2012) Dynamic protein-protein interaction wiring of the human spliceosome. *Mol. Cell* **45,** 567–580
26. Venkatesan, K., Rual, J. F., Vazquez, A., Stelzl, U., Lemmens, I., Hirozane-Kishikawa, T., Hao, T., Zenkner, M., Xin, X., Goh, K. I., Yildirim, M. A., Simonis, N., Heinzmann, K., Gebreab, F., Sahalie, J. M., Cevik, S., Simon, C., Smet, A. S. de, Dann, E., Smolyar, A., Vinayagam, A., Yu, H., Szeto, D., Borick, H., Dricot, A., Klitgord, N., Murray, R. R., Lin, C., Lalowski, M., Timm, J., Rau, K., Boone, C., Braun, P., Cusick, M. E., Roth, F. P., Hill, D. E., Tavernier, J., Wanker, E. E., Barabási, A. L., and Vidal, M. (2009) An empirical framework for binary interactome mapping. *Nat. Methods* **6,** 83–90
27. Vinayagam, A., Stelzl, U., and Wanker, E. E. (2010) Repeated two-hybrid screening detects transient protein–protein interactions. *Theor. Chem. Acc.* **125,** 613–619
28. Worseck, J. M., Grossmann, A., Weimann, M., Hegele, A., and Stelzl, U. (2012) A stringent yeast two-hybrid matrix screening approach for protein–protein interaction discovery. *Meth. Mol. Biol.* **812,** 63–87
29. Rout, M. P., Aitchison, J. D., Suprapto, A., Hjertaas, K., Zhao, Y., and Chait, B. T. (2000) The yeast nuclear pore complex: Composition, architecture, and transport mechanism. *J. Cell Biol.* **148,** 635–651
30. Cronshaw, J. M., Krutchinsky, A. N., Zhang, W., Chait, B. T., and Matunis, M. J. (2002) Proteomic analysis of the mammalian nuclear pore complex. *J. Cell Biol.* **158,** 915–927
31. Brohawn, S. G., and Schwartz, T. U. (2009) Molecular architecture of the Nup84-Nup145C-Sec13 edge element in the nuclear pore complex lattice. *Nat. Struct. Mol. Biol.* **16,** 1173–1177
32. Nagy, V., Hsia, K. C., Debler, E. W., Kampmann, M., Davenport, A. M., Blobel, G., and Hoelz, A. (2009) Structure of a trimeric nucleoporin complex reveals alternate oligomerization states. *Proc. Natl. Acad. Sci. U.S.A.* **106,** 17693–17698
33. Bilokapic, S., and Schwartz, T. U. (2012) 3D ultrastructure of the nuclear pore complex. *Curr. Opin. Cell Biol.* **24,** 86–91
34. Solmaz, SR, Chauhan, R., Blobel, G., and Melčak, I. (2011) Molecular architecture of the transport channel of the nuclear pore complex. *Cell* **147,** 590–602
35. Yoshida, K., Seo, H. S., Debler, E. W., Blobel, G., and Hoelz, A. (2011) Structural and functional analysis of an essential nucleoporin heterotrimer on the cytoplasmic face of the nuclear pore complex. *Proc. Natl. Acad. Sci. U.S.A.* **108,** 16571–16576
36. Leducq, J. B., Charron, G., Diss, G., Gagnon-Arsenault, I., Dubé, A. K., and Landry, C. R. (2012) Evidence for the robustness of protein complexes to inter-species hybridization. *PLoS Genetics* **8,** e1003161
37. Amlacher, S., Sarges, P., Flemming, D., van Noort, V., Kunze, R., Devos, D. P., Arumugam, M., Bork, P., and Hurt, E. (2011) Insight into structure and assembly of the nuclear pore complex by utilizing the genome of a eukaryotic thermophile. *Cell* **146,** 277–289

38. Alber, F., Dokudovskaya, S., Veenhoff, L. M., Zhang, W., Kipper, J., Devos, D., Suprapto, A., Karni-Schmidt, O., Williams, R., Chait, B. T., Rout, M. P., and Sali, A. (2007) Determining the architectures of macromolecular assemblies. *Nature* **450,** 683–694
39. Beck, M., Förster, F., Ecke, M., Plitzko, J. M., Melchior, F., Gerisch, G., Baumeister, W., and Medalia, O. (2004) Nuclear pore complex structure and dynamics revealed by cryoelectron tomography. *Science* **306,** 1387–1390
40. Boehmer, T., Jeudy, S., Berke, I. C., and Schwartz, T. U. (2008) Structural and functional studies of Nup107/Nup133 interaction and its implications for the architecture of the nuclear pore complex. *Molecular Cell* **30,** 721–731
41. Whittle, JR, and Schwartz, T. U. (2009) Architectural nucleoporins Nup157/170 and Nup133 are structurally related and descend from a second ancestral element. *J. Biol. Chem.* **284,** 28442–28452
42. Grandi, P., Emig, S., Weise, C., Hucho, F., Pohl, T., and Hurt, E. C. (1995) A novel nuclear pore protein Nup82p which specifically binds to a fraction of Nsp1p. *J. Cell Biol.* **130,** 1263–1273
43. Fahrenkrog, B., Hübner, W., Mandinova, A., Panté, N., Keller, W., and Aebi, U. (2000) The yeast nucleoporin Nup53p specifically interacts with Nic96p and is directly involved in nuclear protein import. *Mol. Biol. Cell* **11,** 3885–3896
44. Grandi, P., Schlaich, N., Tekotte, H., and Hurt, E. C. (1995) Functional interaction of Nic96p with a core nucleoporin complex consisting of Nsp1p, Nup49p and a novel protein Nup57p. *EMBO J.* **14,** 76–87
45. Bailer, S. M., Balduf, C., Katahira, J., Podtelejnikov, A., Rollenhagen, C., Mann, M., Pante, N., and Hurt, E. (2000) Nup116p associates with the Nup82p-Nsp1p-Nup159p nucleoporin complex. *J. Biol. Chem.* **275,** 23540–23548
46. Stuwe, T., Borzyskowski, L. S. von, Am Davenport, and Hoelz, A. (2012) Molecular basis for the anchoring of proto-oncoprotein Nup98 to the cytoplasmic face of the nuclear pore complex. *J. Mol. Biol.* **419,** 330–346
47. Schlaich, N. L., Häner, M., Lustig, A., Aebi, U., and Hurt, E. C. (1997) In vitro reconstitution of a heterotrimeric nucleoporin complex consisting of recombinant Nsp1p, Nup49p, and Nup57p. *Mol. Biol. Cell* **8,** 33–46
48. Ori, A., Banterle, N., Iskar, M., Andrés-Pons, A., Escher, C., Khanh, B. H., Sparks, L., Solis-Mezarino, V., Rinner, O., Bork, P., Lemke, E. A., and Beck, M. (2013) Cell type-specific nuclear pores: A case in point for context-dependent stoichiometry of molecular machines. *Mol. Syst. Biol.* **9,** 648
49. Jerabek-Willemsen, M., Wienken, C. J., Braun, D., Baaske, P., and Duhr, S. (2011) Molecular interaction studies using microscale thermophoresis. *Assay Drug Develop. Tech.* **9,** 342–353
50. Jerabek-Willemsen, M., André, T., Wanner, R., Roth, H. M., Duhr, S., Baaske, P., and Breitsprecher, D. (2014) MicroScale thermophoresis: Interaction analysis and beyond. *J. Mol. Structure* **1077,** 101–113
51. Ruthenburg, A. J., Li, H., Patel, D. J., and Allis, C. D. (2007) Multivalent engagement of chromatin modifications by linked binding modules. *Nature Rev.* **8,** 983–994
52. Neumann, N., Lundin, D., and Poole, A. M. (2010) Comparative genomic evidence for a complete nuclear pore complex in the last eukaryotic common ancestor. *PloS One* **5,** e13241
53. Bilokapic, S., and Schwartz, T. U. (2012) Molecular basis for Nup37 and ELY5/ELYS recruitment to the nuclear pore complex. *Proc. Natl. Acad. Sci. U.S.A.* **109,** 15241–15246
54. Michnick, S. W., Ear, P. H., Manderson, E. N., Remy, I., and Stefan, E. (2007) Universal strategies in research and drug discovery based on protein-fragment complementation assays. *Nature Rev.* **6,** 569–582
55. Kerppola, T. K. (2009) Visualization of molecular interactions using bimolecular fluorescence complementation analysis: Characteristics of protein fragment complementation. *Chem. Soc. Rev.* **38,** 2876–2886
56. Miller, K. E., Kim, Y., Huh, W. K., and Park, H. O. (2015) Bimolecular Fluorescence Complementation (BiFC) Analysis: Advances and recent applications for genome-wide interaction studies. *J. Mol. Biol.* **427,** 2039–2055
57. Beck, M., Lucić, V., Förster, F., Baumeister, W., and Medalia, O. (2007) Snapshots of nuclear pore complexes in action captured by cryo-electron tomography. *Nature* **449,** 611–615
58. Frenkiel-Krispin, D., Maco, B., Aebi, U., and Medalia, O. (2010) Structural analysis of a metazoan nuclear pore complex reveals a fused concentric ring architecture. *J. Mol. Biol.* **395,** 578–586
59. Maimon, T., Elad, N., Dahan, I., and Medalia, O. (2012) The human nuclear pore complex as revealed by cryo-electron tomography. *Structure* **20,** 998–1006
60. Eibauer, M., Pellanda, M., Turgay, Y., Dubrovsky, A., Wild, A., and Medalia, O. (2015) Structure and gating of the nuclear pore complex. *Nature Commun.* **6,** 7532
61. Loïodice, I., Alves, A., Rabut, G., van Overbeek, M., Ellenberg, J., Sibarita, J. B., and Doye, V. (2004) The entire Nup107–160 complex, including three new members, is targeted as one entity to kinetochores in mitosis. *Mol. Biol. Cell* **15,** 3333–3344
62. Rasala, B. A., Orjalo, A. V., Shen, Z., Briggs, S., and Forbes, D. J. (2006) ELYS is a dual nucleoporin/kinetochore protein required for nuclear pore assembly and proper cell division. *Proc. Natl. Acad. Sci. U.S.A.* **103,** 17801–17806
63. Kampmann, M., and Blobel, G. (2009) Three-dimensional structure and flexibility of a membrane-coating module of the nuclear pore complex. *Nature Struct. Mol. Biol.* **16,** 782–788
64. Hsia, K. C., Stavropoulos, P., Blobel, G., and Hoelz, A. (2007) Architecture of a coat for the nuclear pore membrane. *Cell* **131,** 1313–1326
65. Shi, Y., Fernandez-Martinez, J., Tjioe, E., Pellarin, R., Kim, S. J., Williams, R., Schneidman-Duhovny, D., Sali, A., Rout, M. P., and Chait, B. T. (2014) Structural characterization by cross-linking reveals the detailed architecture of a coatomer-related heptameric module from the nuclear pore complex. *Mol. Cell. Proteomics* **13,** 2927–2943
66. Bar-Peled, L., Chantranupong, L., Cherniack, A. D., Chen, W. W., Ottina, K. A., Grabiner, B. C., Spear, E. D., Carter, S. L., Meyerson, M., and Sabatini, D. M. (2013) A Tumor suppressor complex with GAP activity for the Rag GTPases that signal amino acid sufficiency to mTORC1. *Science* **340,** 1100–1106
67. Schrader, N., Stelter, P., Flemming, D., Kunze, R., Hurt, E., and Vetter, I. R. (2008) Structural basis of the nic96 subcomplex organization in the nuclear pore channel. *Mol. Cell* **29,** 46–55
68. Knockenhauer, K. E., and Schwartz, T. U. (2016) The nuclear pore complex as a flexible and dynamic gate. *Cell* **164,** 1162–1171
69. Lupu, F., Alves, A., Anderson, K., Doye, V., and Lacy, E. (2008) Nuclear pore composition regulates neural stem/progenitor cell differentiation in the mouse embryo. *Develop. Cell* **14,** 831–842
70. Lowe, A. R., Tang, J. H., Yassif, J., Graf, M., Huang, W. Y., Groves, J. T., Weis, K., and Liphardt, J. T. (2015) Importin-beta modulates the permeability of the nuclear pore complex in a Ran-dependent manner. *eLife* **4**
71. Stefan, E., Malleshaiah, M. K., Breton, B., Ear, P. H., Bachmann, V., Beyermann, M., Bouvier, M., and Michnick, S. W. (2011) PKA regulatory subunits mediate synergy among conserved G-protein-coupled receptor cascades. *Nature Commun.* **2,** 598
72. Orchard, S., Ammari, M., Aranda, B., Breuza, L., Briganti, L., Broackes-Carter, F., Campbell, N. H., Chavali, G., Chen, C., del-Toro, N., Duesbury, M., Dumousseau, M., Galeota, E., Hinz, U., Iannuccelli, M., Jagannathan, S., Jimenez, R., Khadake, J., Lagreid, A., Licata, L., Lovering, R. C., Meldal, B., Melidoni, A. N., Milagros, M., Peluso, D., Perfetto, L., Porras, P., Raghunath, A., Ricard-Blum, S., Roechert, B., Stutz, A., Tognolli, M., van Roey, K., Cesareni, G., and Hermjakob, H. (2014) The MIntAct project—IntAct as a common curation platform for 11 molecular interaction databases. *Nucleic Acids Res.* **42,** D358–D363